

# On the Role of Sparsity and DAG Constraints for Learning Linear DAGs

Ignavier Ng<sup>1</sup>

AmirEmad Ghassami<sup>2</sup>

Kun Zhang<sup>3</sup>

<sup>1</sup>University of Toronto, Toronto, ON M5S, Canada

<sup>2</sup>University of Illinois at Urbana-Champaign, Urbana, IL 61801, USA

<sup>3</sup>Carnegie Mellon University, Pittsburgh, PA 15213, USA

## Abstract

Learning graphical structure based on Directed Acyclic Graphs (DAGs) is a challenging problem, partly owing to the large search space of possible graphs. Recently, NOTEARS (Zheng et al., 2018) formulates the structure search problem as a continuous optimization task using the least squares objective and a proper characterization of DAGs. However, the formulation requires a hard DAG constraint and may lead to optimization difficulties. In this paper, we study the asymptotic roles of the sparsity and DAG constraints for learning DAG models in the linear Gaussian and non-Gaussian cases, and investigate their usefulness in the finite sample regime. Based on the theoretical results, we formulate a likelihood-based score function, and show that one only has to apply sparsity and DAG regularization terms to recover the underlying DAGs. This leads to an unconstrained optimization problem that is much easier to solve. Using gradient-based optimization and GPU acceleration, our procedure can easily handle thousand of nodes while retaining a high accuracy. Extensive experiments validate the effectiveness of our proposed method and show that the DAG-regularized likelihood objective is indeed favorable over the least squares one with the hard DAG constraint.

## 1 Introduction

Learning graphical structure from data based on Directed Acyclic Graphs (DAGs) is a fundamental problem in machine learning, with applications in many areas such as biology (Sachs et al., 2005) and healthcare (Lucas et al., 2004). It is clear that the learned graphical models may not have causal interpretations (Pearl, 2009; Spirtes et al., 2000). However, they provide a compact, yet flexible, way to decompose the joint distribution. Under further conditions, these graphical models may have causal interpretations or be converted to representations (e.g., Markov equivalence classes) that have causal interpretations.

Two major classes of structure learning methods are constraint-based and score-based methods. Constraint-based methods, including PC (Spirtes and Glymour, 1991) and FCI (Spirtes et al., 1995; Colombo et al., 2011), utilize conditional independence tests to recover the Markov equivalence class under the faithfulness assumption. On the other hand, score-based methods cast the structure learning problem as optimizing for a certain score function (Heckerman et al., 1995; Chickering, 2002; Teyssier and Koller, 2012; Solus et al., 2017). Due to the large search space of possible graphs (Chickering, 1996; He et al., 2015), most score-based methods rely on local heuristics, such as GES (Chickering, 2002).

Recently, Zheng et al. (2018) introduce the NOTEARS approach which formulates the structure search problem as a continuous optimization task, leveraging a characterization of DAGs. NOTEARS is specifically developed for linear DAG models, yet subsequent extensions apply neural networks to modeling nonlinear relationships (Kalainathan et al., 2018; Yu et al., 2019; Ng et al., 2019a,b; Lachapelle et al., 2020; Zheng et al., 2020). Other variants include DYNOTEARS (Pamfil et al., 2020) that focuses on time series data, and (Zhu et al., 2020) that uses reinforcement learning to search for the optimal DAGs, which does not require the score function be smooth. NOTEARS and the majority of its extensions adopt the least squares objective,

which is related to but does not directly maximize the data likelihood. Furthermore, their formulations require a hard DAG constraint which may lead to optimization difficulties.

In this work, we investigate whether such a hard DAG constraint and another widely used constraint, known as sparsity of the graph, are necessary for learning DAGs. As a by-product, we develop a likelihood-based structure learning method with continuous optimization, called *Gradient-based Optimization of dag-regularized Likelihood for learning linEar dag Model* (GOLEM). Our contributions are as follows:

- We compare the differences between the regression-based and likelihood-based objectives for learning linear DAGs.
- We study the asymptotic roles of the sparsity and DAG constraints in the general linear Gaussian case, as well as other specific cases including the linear non-Gaussian model and linear Gaussian model with equal noise variances. We also investigate their usefulness in the finite sample regime.
- Based on the theoretical results, we formulate a likelihood-based score function, and show that one only has to apply sparsity and DAG regularization terms (i.e., soft constraints) to recover the underlying DAGs, which removes the need for a hard DAG constraint<sup>1</sup>(Zheng et al., 2018). This leads to an unconstrained optimization problem that is much easier to solve.
- We demonstrate the effectiveness of our DAG-regularized likelihood objective through extensive experiments and an analysis on the bivariate linear Gaussian model.

The rest of the paper is organized as follows: We review the linear DAG model and the NOTEARS approach in Section 2. We then discuss the asymptotic roles of sparsity and DAG constraints under different settings in Section 3. Based on the theoretical results, we formulate a regularized likelihood-based score function in Section 4, and compare it to NOTEARS and the least squares objective. The experiment results in Section 5 verify our theoretical results and the effectiveness of our method. Finally, we conclude our work in Section 6. All the proofs and derivations are given in the supplementary materials.

## 2 Background

### 2.1 Linear DAG Model

As a general rule throughout, we refer to a random variable with a capital letter (e.g.  $X$ ), and its particular value with a lowercase letter (e.g.  $x$ ). A DAG model defined on a set of random variables  $X := [X_1, \dots, X_d]^\top$  consists of (1) a DAG  $G = (V(G), E(G))$  that encodes a set of conditional independence assertions among the variables, and (2) the joint distribution  $P(X)$  (with density function  $p_X(\cdot)$ ) that is Markov with respect to  $G$ , which factors as  $P(X) = \prod_{i=1}^d P(X_i | X_{\text{pa}(i)})$ , where  $\text{pa}(i) := \{j \in V(G) : X_j \rightarrow X_i \in E(G)\}$  denotes the set of parents of  $X_i$  in  $G$ . In this paper, we focus on the linear DAG models that can be equivalently represented by a set of linear Structural Equation Models (SEMs), in which each variable obey the model  $X_i = W_i^\top X + Z_i$ , where  $W_i$  is a coefficient vector, and  $Z_i$  is the noise variable corresponding to variable  $X_i$ . In matrix form, the linear DAG model is given by  $X = W^\top X + Z$ , where  $W = [W_1 | \dots | W_d]$  is a weighted adjacency matrix, and  $Z = [Z_1, \dots, Z_d]^\top$  is a noise vector with independent entries. The structure of  $G$  is defined by the non-zero coefficients in  $W$ , i.e.,  $X_j \rightarrow X_i \in E(G)$  if the coefficient in  $W_i$  corresponding to  $X_j$  is non-zero. Given i.i.d. samples  $\mathbf{x} = \{x^{(k)}\}_{k=1}^n$  generated from the joint distribution  $P(X)$ , our goal is to infer the unknown matrix  $W$ , from which we may recover the DAG  $G$  (or vice versa).

### 2.2 The NOTEARS approach

Zheng et al. (2018) formulate the structure search problem as a continuous optimization task, by leveraging a proper algebraic characterization of DAGs via the trace exponential function. It solves the linear DAG model

---

<sup>1</sup>Using constrained optimization, the hard DAG constraint would strictly enforce the estimated graph to be acyclic (up to numerical precision), which is stronger than a DAG regularization term (i.e., soft constraint).

using *least squares* objective with  $\ell_1$  regularization and a hard DAG constraint. The optimization problem can be solved using the augmented Lagrangian method (Bertsekas, 1999), followed by a thresholding step on the estimated entries.

In practice, the hard DAG constraint requires careful fine-tuning on the augmented Lagrangian parameters (Birgin et al., 2005, 2012; Nie et al., 2004). It may also exhibit unstable behaviors when the penalty terms are increased to relatively large values. Moreover, minimizing the least squares objective is related to but does not directly maximize the data likelihood because it is derived from the *conditional* Gaussian likelihood. With  $\ell_1$  regularization, this corresponds to a multiple-output lasso problem (Tibshirani, 1996), where the  $\ell_1$  regularization merely induces sparsity, and does not enforce any shared structure among the regression coefficients of different variables. Thus, the least squares objective is *decomposable* into  $d$  independent regression problems. By contrast, our work aims at optimizing for the *joint* likelihood, and requires only sparsity and DAG regularization terms.

### 3 Asymptotic Roles of Sparsity and DAG Constraints

In this section, we study the asymptotic roles of the sparsity and DAG constraints. Specifically, we aim to investigate with different model classes, whether one should consider the DAG constraint as a hard one or a regularization term, and what exactly one benefits from the sparsity constraint. We consider a score-based structure learning procedure which optimizes the following score function:

$$\mathcal{S}(W; \mathbf{x}) := -\mathcal{L}(W; \mathbf{x}) + R_{\text{sparse}}(W) + R_{\text{DAG}}(W), \quad (1)$$

where  $\mathcal{L}(W; \mathbf{x})$  is the likelihood objective,  $R_{\text{sparse}}(W)$  is a regularization term encouraging sparsity, i.e., having fewer edges, and  $R_{\text{DAG}}(W)$  is a regularization term encouraging DAGness on  $W$ .<sup>2</sup> It is worth noting that the sparsity (or frugality) constraint has been exploited to find the DAG or its Markov equivalence class with as few edges as possible, searching in the space of DAGs or equivalence classes. In particular, permutation-based estimation methods have been developed to find the sparsest DAG across possible permutations of the variables (Solus et al., 2017; Raskutti and Uhler, 2018). This type of methods may benefit from smart optimization procedures, but inevitably they involve combinatorial optimization. Different from previous work, in this paper we do not necessarily constrain the search procedure in the space of DAGs in a hard manner, but the estimated graph may still end up with a DAG if the ground truth is acyclic.

We will describe our specific choices of the regularization functions in Section 4. Throughout the paper, we assume that the ground truth structure is a DAG. We are concerned with two different situations. One is the general linear Gaussian case (i.e., assuming non-equal noise variances), for which it is known that the underlying DAG structure is not identifiable from the data distribution only (Koller and Friedman, 2009). In the other situation, the underlying DAG model is asymptotically identifiable from the data distribution itself, with or without constraining the search space to be the class of DAGs.

#### 3.1 General Linear Gaussian Case

We first study the class of structures for which the sparsity regularization  $R_{\text{sparse}}(W)$  is enough for the Maximum Likelihood Estimator (MLE) to asymptotically learn a DAG equivalent to the ground truth DAG, i.e., the DAG regularization  $R_{\text{DAG}}(W)$  is not needed. Then we show that for the general structures, adding  $R_{\text{DAG}}(W)$  guarantees learning a DAG equivalent to the ground truth DAG. We first require a notion of equivalence to be able to investigate the consistency of the approach.

Ghassami et al. (2019) introduced a notion of equivalence among directed graphs, called quasi equivalence, as follows: For a directed graph  $G$ ,<sup>3</sup> define the distribution set of  $G$ , denoted by  $\Theta(G)$ , as the set of all precision matrices (equivalently, distributions) that can be generated by  $G$  for different choices of exogenous noise variances and edge weights in  $G$ . Define a *distributional constraints* as any equality or inequality

<sup>2</sup>The analysis in this section also applies to a hard DAG constraint.

<sup>3</sup>In this section the notation  $G$  can refer to both acyclic and cyclic directed graphs.

constraint imposed by  $G$  on the entries of precision matrix  $\Theta$ . Also define a *hard constraint* as a distributional constraint for which the set of the values satisfying that constraint is Lebesgue measure zero over the space of the parameters involved in the constraint. The set of hard constraints of a directed graph  $G$  is denoted by  $H(G)$ . Note that the notion of hard constraint here is different from the hard DAG constraint used by [Zheng et al. \(2018\)](#).

**Definition 1 (Quasi Equivalence).** *Let  $\theta_G$  be the set of linearly independent parameters needed to parameterize any distribution  $\Theta \in \Theta(G)$ . For two directed graphs  $G_1$  and  $G_2$ , let  $\mu$  be the Lebesgue measure defined over  $\theta_{G_1} \cup \theta_{G_2}$ .  $G_1$  and  $G_2$  are quasi equivalent if  $\mu(\theta_{G_1} \cap \theta_{G_2}) \neq 0$ .*

Roughly speaking, two directed graphs are quasi equivalent if the set of distributions that they can both generate has a non-zero Lebesgue measure. See Appendix A for an example of quasi equivalence. Definition 1 implies that if directed graphs  $G_1$  and  $G_2$  are quasi equivalent they share the same hard constraints.

The following two assumptions are required for the task of structure learning from observational data.

**Assumption 1 (G-faithfulness Assumption).** *A distribution  $\Theta$  is generalized faithful (g-faithful) to structure  $G$  if  $\Theta$  satisfies a hard constraint  $\kappa$  if and only if  $\kappa \in H(G)$ . We say that the g-faithfulness assumption is satisfied if the generated distribution is g-faithful to the ground truth structure.*

**Assumption 2.** *Let  $E(G)$  be the set of edges of  $G$ . For a DAG  $G^*$ , and a directed graph  $\hat{G}$ , we have the following statements.*

- (a) *If  $|E(\hat{G})| \leq |E(G^*)|$ , then  $H(\hat{G}) \not\subseteq H(G^*)$ .*
- (b) *If  $|E(\hat{G})| < |E(G^*)|$ , then  $H(\hat{G}) \not\subseteq H(G^*)$ .*

Note that Assumption 1 is an extension of the well-known faithfulness assumption ([Spirtes et al., 2000](#)). The intuition behind Assumption 2 is that in DAGs all the parameters can be chosen independently. Hence, each parameter introduces an independent dimension to the distribution space. Therefore, if a DAG and another directed graph  $\hat{G}$  have the same number of edges, then the distribution space of the DAG cannot be a strict subset with lower dimension of the distribution space of  $\hat{G}$ . Note that the assumption holds if  $\hat{G}$  is also a DAG. [Ghassami et al. \(2019\)](#) showed that the g-faithfulness assumption is a mild assumption in the sense that the Lebesgue measure of the distributions not g-faithful to the ground truth is zero, and showed that under Assumption 1 and a condition similar to Assumption 2, the underlying directed graph can be identified up to quasi equivalence and proposed an algorithm to do so.

In the following, we first consider the case that the DAG regularization  $R_{DAG}(W)$  term in expression (1) is not needed. The following condition is required for this case.

**Assumption 3 (Triangle Assumption).** *A DAG satisfies the triangle assumption if it does not have any triangles (i.e., 3-cycles) in its skeleton.*

As an example, any polytree satisfies the triangle assumption.

**Theorem 1.** *If the underlying DAG satisfies Assumptions 1-3, a sparsity regularized MLE asymptotically returns a DAG quasi equivalent to the ground truth DAG.*

If we relax the triangle assumption, then the optimizer of  $-\mathcal{L}(W; \mathbf{x}) + R_{sparse}(W)$  can be cyclic as well. However, the following theorem shows that even in this case, some optimizers are still acyclic.

**Theorem 2.** *If the underlying DAG satisfies Assumptions 1 and 2, the output of sparsity regularized MLE asymptotically has the same number of edges as the ground truth.*

This motivates us to add the DAG regularization term  $R_{DAG}(W)$  to the score function (1) to prefer a DAG solution to cyclic solution with the same number of edges.

**Corollary 1.** *If the underlying DAG satisfies Assumptions 1 and 2, a sparsity and DAG regularized MLE asymptotically returns a DAG quasi equivalent to the ground truth DAG.*

The proofs for Theorem 1 and 2 are given in Appendix B. Corollary 1 implies that under mild assumption, likelihood-based objectives with sparsity and DAG regularization terms are able to recover a DAG up to quasi equivalence in the general linear Gaussian case, as verified by the simulations in Section 5.1.

### 3.2 With Identifiable Linear DAG Model

In a different line of research, linear DAG models may be identifiable under specific assumptions. Suppose the ground truth is a DAG. There are two types of identifiability results for the underlying DAG structure. One does not require the constraint that the search space is the class of DAGs; a typical example is the Linear Non-Gaussian Acyclic Model (LiNGAM) (Shimizu et al., 2006), where at most one of the noise terms (including root cause variables) follows the Gaussian distribution. In this case, it was shown that as the sample size goes to infinity, among all directed graphical models that are acyclic or cyclic, only the underlying true graphical model, which is a DAG, can generate exactly the given data distribution, thanks to the identifiability results of the Independent Component Analysis (ICA) problem (Hyvärinen et al., 2001). As a consequence, asymptotically speaking, given observational data generated by the LiNGAM, we do not need to enforce the sparsity or DAG constraint in the estimation procedure that maximizes the data likelihood, and the estimated graphical model will converge to the ground truth DAG. However, on finite samples, one still benefits from enforcing the DAG and sparsity constraints, by incorporating corresponding regularization terms: because of random estimation errors, the linear coefficients whose true values are zero may have non-zero estimated values in the maximum likelihood estimate, and the constraints help set them to zero.

In contrast, the other type of identifiable linear DAG model constrains the estimated graph to be in the class of DAGs. An example is the linear SEMs with equal noise variances (Peters and Bühlmann, 2013), in which the variables are generated from their parents and noise, according to the DAG structure, and the noise terms in all variables have the same variance. In the proof of the identifiability result (Peters and Bühlmann, 2013, Theorem 1), it shows that when the sample size is infinity, no other DAG structure can generate the same distribution. In theory, it is unclear whether any cyclic graph can generate the same distribution; however, we strongly believe that in this identifiability result, one has to enforce DAGness on the search space or sparsity of the edges, as suggested by our empirical results (Section 5.1) and an analysis on the bivariate case (Proposition 1).

Note that whether one can benefit from the above identifiability results depends on the form of the likelihood function. If it does not take into account the additional assumptions that give rise to identifiability, but relies on the general linear Gaussian model, then the analysis in Section 3.1 still applies.

## 4 GOLEM: A Continuous Likelihood-Based Score Function

The theoretical results in Section 3 suggest that sparsity and DAG regularizations suffice to recover the underlying DAGs, under mild assumption. In this section, we formulate a continuous likelihood-based score function based on these regularization terms, and describe the post-processing step and computational complexity. We then compare the resulting method with NOTEARS and the least squares objective.

### 4.1 Maximum Likelihood Objective with DAG regularization

We formulate a score-based method to maximize the *joint* likelihood of a linear Gaussian model, with a focus on continuous optimization. The joint distribution  $P(X)$  follows multivariate Gaussian distribution, which gives the following maximum likelihood objective in the general linear Gaussian case:

$$\mathcal{L}_1(W; \mathbf{x}) := -\frac{1}{2} \sum_{i=1}^d \log \left( \sum_{k=1}^n (x_i^{(k)} - W_i^\top x^{(k)})^2 \right) + \log |\det(I - W)|. \quad (2)$$

If one further assumes that the noise variances are equal (although they may be non-equal), it becomes

$$\mathcal{L}_2(W; \mathbf{x}) := -\frac{d}{2} \log \left( \sum_{i=1}^d \sum_{k=1}^n (x_i^{(k)} - W_i^\top x^{(k)})^2 \right) + \log |\det(I - W)|. \quad (3)$$

A derivation is provided in Appendix C. The objectives above are denoted as likelihood-NV and likelihood-EV, respectively. These objectives further give rise to the Bayesian Information Criterion (BIC) scores (Schwarz,

1978) (excluding complexity penalty term) with non-equal and equal noise variances, respectively, under linear Gaussian setting. In principle, one should use (a function of) the number of edges to assess the structure complexity, such as the  $\ell_0$  penalty from BIC score (Van de Geer and Bühlmann, 2013; Raskutti and Uhler, 2018). One may also fine-tune the penalization coefficient, if needed.

However, it is difficult to optimize such score in practice (e.g., GES (Chickering, 2002) adopts greedy search in the discrete space). To enable efficient continuous optimization, we use the  $\ell_1$  penalty for approximation. Although the  $\ell_1$  penalty has been widely used in regression tasks (Meinshausen and Bühlmann, 2006; Tibshirani, 1996) to find sparse precision or covariance matrices (Friedman et al., 2008), it has been rarely used to directly penalize the likelihood function in linear Gaussian case (Aragam and Zhou, 2015). With  $\ell_1$  and DAG regularization terms, the *unconstrained* optimization problems of our score functions are

$$\min_W \mathcal{S}_i(W; \mathbf{x}) := -\mathcal{L}_i(W; \mathbf{x}) + \lambda_1 \|W\|_1 + \lambda_2 h(W), \quad (4)$$

where  $i = 1, 2$ ,  $\lambda_1$  and  $\lambda_2$  are the regularization coefficients, and  $h(W) := \text{tr}(e^{W \odot W}) - d$  is the characterization of DAGness proposed by Zheng et al. (2018). It is possible to use the improved characterization given by Yu et al. (2019), which is left for future work. The score functions  $\mathcal{S}_i(W; \mathbf{x})$ ,  $i = 1, 2$  correspond respectively to the likelihood-NV and likelihood-EV objectives with sparsity and DAG regularization terms, which are denoted as GOLEM-NV and GOLEM-EV, respectively.

Similar to Zheng et al. (2018), the main advantage of our proposed score functions is that continuous method can be applied to solve the optimization problem, such as first-order (e.g., gradient descent) or second-order (e.g., L-BFGS (Byrd et al., 2003)) methods. Nevertheless, it inherits the difficulties of non-convexity, owing to the log determinant (LogDet) and DAG regularization terms, indicating that the problem can only be solved to stationarity. Nonetheless, the empirical results in Section 5 demonstrate that this leads to competitive performance in practice. Here we adopt gradient descent method implemented in Tensorflow (Abadi et al., 2016) with GPU acceleration and automatic differentiation. More details regarding the optimization procedure are described in Appendix E.

**Initialization Scheme** In practice, the optimization problem given by GOLEM-NV is susceptible to local solutions. To remedy this, we find that initializing the optimization of GOLEM-NV with the solution returned by GOLEM-EV dramatically helps avoid undesired solutions in our experiments.

## 4.2 Post-Processing

Due to finite samples and non-convexity, the local solutions obtained may contain several entries near zero and may not be exactly acyclic. We set a small threshold  $\omega$  at 0.3, as in (Zheng et al., 2018), to remove edges with absolute weights smaller than  $\omega$ . The key idea is to “round” the numerical solution into a discrete graph, and also remove false discoveries. If the thresholded graph is not a DAG, we remove edges iteratively starting from the lowest absolute weights, until a DAG is obtained. In other words, one may gradually increase the threshold  $\omega$  until  $W$  is acyclic. This heuristic is made possible by virtue of the DAG regularization, as it pushes the cycle-inducing edges to small values.

## 4.3 Computational Complexity

First-order method involves gradient evaluation; the derivative of the LogDet term from the score functions  $\mathcal{S}_i(W; \mathbf{x})$ ,  $i = 1, 2$  is given by

$$\nabla_W \log |\det(I - W)| = (I - W)^{-\top}.$$

This implies that  $\mathcal{S}_i(W; \mathbf{x})$  and its gradient involve evaluating the LogDet and matrix inverse terms. Similar to matrix exponential (Al-Mohy and Higham, 2009), both operations require  $\mathcal{O}(d^3)$  costs (Strassen, 1969; Han et al., 2015), with implementations readily available in multiple scientific computing frameworks (Abadi et al., 2016). Thus, gradient-based optimization of problem (4) would incur  $\mathcal{O}(d^3)$  cost per iteration, similar to (Zheng et al., 2018). Nonetheless, the experiments in Section 5.4 demonstrate that the optimization could benefit from GPU acceleration, showing that the cubic evaluation cost is not a major concern.

## 4.4 Connection with NOTEARS and Least Squares Objective

It is instructive to compare the likelihood-EV objective (3) to the least squares, by rewriting (3) as

$$\mathcal{L}_2(W; \mathbf{x}) = -\frac{d}{2} \log (\ell(W; \mathbf{x})) + \log |\det(I - W)| - \frac{d}{2} \log 2n, \quad (5)$$

where  $\ell(W; \mathbf{x}) := \frac{1}{2n} \sum_{i=1}^d \sum_{k=1}^n (x_i^{(k)} - W_i^T x^{(k)})^2$  is the least squares objective. One observes that the main difference lies in the LogDet term. As discussed in Section 2.2, without the LogDet term, the least squares objective corresponds to a multiple-output lasso problem, which is decomposable into  $d$  independent regression tasks. Thus, least squares objective tends to introduce cycles in the estimated graphs (see Proposition 1 for an analysis on the bivariate case). Consider two variables  $X_i$  and  $X_j$  that are conditionally dependent given any subset of the remaining variables, then one of them is useful in predicting the other. That is, when minimizing least squares objective for one of them, the other variable will tend to have non-zero coefficient. If one considers those coefficients as weights of the graph, then the graph will have cycles. By contrast, the likelihood-based objective has an additional LogDet term that enforces shared structure between the regression coefficients of different variables. We have the following lemma regarding the LogDet term.

**Lemma 1.** *If a weighted matrix  $W \in \mathbb{R}^{d \times d}$  corresponds to a DAG, then*

$$\log |\det(I - W)| = 0.$$

Lemma 1 partly explains why a hard DAG constraint is needed by the least squares (Zheng et al., 2018), as its global optimizer(s) is (are) identical to the likelihood-EV objective if the search space over  $W$  is constrained to DAGs. However, the hard DAG constraint may lead to optimization difficulties, as it may exhibit unstable behaviors for large penalty terms (cf. Section 2.2). With a proper scoring criterion, the ground truth DAG should maximise the criterion, thus the hard DAG constraint could be avoided. As suggested by our theoretical results, using likelihood-based objective, one may simply treat the constraint as regularization term, which is much easier to solve. The experiments in Section 5 show that our proposed DAG-regularized likelihood yields better performance in most settings.

To illustrate our arguments above, we provide an example in the bivariate case. We consider the linear Gaussian model with ground truth DAG  $G : X_1 \rightarrow X_2$  and equal noise variances, characterized by the following weighted adjacency matrix and noise covariance matrix:

$$W_0 = \begin{bmatrix} 0 & w_0 \\ 0 & 0 \end{bmatrix}, \Omega = \begin{bmatrix} \sigma^2 & 0 \\ 0 & \sigma^2 \end{bmatrix}, w_0 \neq 0. \quad (6)$$

We have the following proposition in the asymptotic case, with a proof given in Appendix D.

**Proposition 1.** *Suppose  $X$  is drawn from a linear DAG model in Eq. (6). Then, asymptotically,*

- (i)  *$W_0$  is the unique optimizer of the least squares objective under a hard DAG constraint, but without the DAG constraint, the least squares objective returns a cyclic graph.*
- (ii)  *$W_0$  is the unique optimizer of the likelihood-EV objective (3) under  $\ell_1$  or DAG regularization.*

Therefore, without the DAG constraint, the least squares method never returns a DAG, while the likelihood objective does not favor cyclic over acyclic structures. This statement is also true in general: as long as a structure, be cyclic or acyclic, can generate a distribution, it can be the output of a likelihood score asymptotically. However, the least squares objective without constraint never returns an acyclic graph.

Furthermore, Proposition 1 implies that both objectives produce asymptotically correct results in the bivariate case, under different conditions. Nevertheless, the condition required by the likelihood-EV objective (GOLEM-EV) is looser than that of the least squares (NOTEARS), as it requires only a slight sparsity or DAG regularization term to recover the underlying DAG. This bivariate example illustrates our asymptotic study in Section 3 that GOLEM is consistent in the general case, showing that the likelihood-based objective is favorable over the regression-based one that requires a hard DAG constraint.

## 5 Experiments

We first conduct experiments with increasing sample size to verify our theoretical results (Section 5.1). To validate the effectiveness of our resulting score-based method, we compare it to several baselines in both identifiable (Section 5.2) and non-identifiable (Section 5.3) cases. The baselines include FGS (Ramsey et al., 2017), PC (Spirtes and Glymour, 1991), DirectLiNGAM (Shimizu et al., 2011), NOTEARS-L1 and NOTEARS (Zheng et al., 2018). In Section 5.4, we conduct experiments on large graphs to analyze the efficiency and scalability of the proposed method. We then provide a sensitivity analysis in Section 5.5 to investigate the robustness of different methods. Lastly, we apply our method to real data (Section 5.6). The implementation details of baselines and hyperparameters of our method are described in Appendix F.1 and E, respectively.

We use a similar experiment setup as in (Zheng et al., 2018). The ground truth DAG is generated from either *Erdős-Rényi* (ER) or *Scale Free* (SF) graphs, with different graph sizes and edge density. We use ER4 to denote an ER graph with on average  $4d$  edges, likewise for the others. Unless otherwise stated, we construct the weight matrix  $W$  by assigning uniformly random edge weights, and simulate  $n = 1000$  samples based on the linear DAG model with different noise types. We evaluate the estimated graphs using Structural Hamming Distance (SHD), True Positive Rate (TPR), False Discovery Rate (FDR) and SHD-CPDAG, averaged over 12 random seeds. Detailed explanation of the experiment setup and metrics can be found in Appendix F.2 and F.3, respectively.

### 5.1 Asymptotic Roles of Sparsity and DAG Constraints

We investigate the asymptotic roles of  $\ell_1$  and DAG regularizations in both identifiable and non-identifiable cases, by considering the linear Gaussian model with equal (*Gaussian-EV*) and non-equal (*Gaussian-NV*) noise variances, respectively. For *Gaussian-EV*, we experiment with the following variations: GOLEM-EV (with both  $\ell_1$  and DAG regularizations), GOLEM-EV-L1 (with only  $\ell_1$  regularization) and GOLEM-EV-Plain (without any regularization term), likewise for GOLEM-NV, GOLEM-NV-L1 and GOLEM-NV-Plain in the case of *Gaussian-NV*. Experiments are conducted on ER1 and ER4 graphs, each with sample size  $n \in \{100, 300, 1000, 3000, 10000\}$ .

Due to space limit, the results are shown in Appendix G.1. For the *Gaussian-EV* case, when the sample size is large, the graphs estimated by both GOLEM-EV and GOLEM-EV-L1 are close to the ground truth DAGs, whereas GOLEM-EV-Plain has poor results without any regularization term. Notice also that the gap between GOLEM-EV-L1 and GOLEM-EV decreases with more samples, indicating that sparsity regularization seems to be sufficient to recover the underlying DAGs in the asymptotic case. However, this is not the case for *Gaussian-NV*, as the performance of GOLEM-NV-L1 degrades without the DAG regularization term. These observations are consistent with our asymptotic study: (1) For the general *Gaussian-NV* case, although Theorem 1 states that sparsity regularization is sufficient to recover the underlying DAGs, the triangle assumption is not satisfied in this simulation. Corollary 1 has mild assumption which applies here, implying that both sparsity and DAG regularizations are required. (2) When the noise variances are assumed to be equal, i.e., the *Gaussian-EV* case, Section 3.2 states that either sparsity or DAG regularization could help to recover the underlying DAGs, thanks to the identifiability results. Nevertheless, DAG regularization is still very helpful in practice, especially on smaller sample sizes and denser graphs.

### 5.2 Numerical Results: Identifiable Cases

We examine the structure learning performance in the identifiable cases. In particular, we simulate {ER1, ER2, ER4, SF1, SF2, SF4} graphs with  $d \in \{10, 20, 50, 100\}$  nodes, based on different noise types: *Gaussian-EV*, *Exponential* and *Gumbel*.

For better visualization, the SHDs and TPRs of gradient-based methods (i.e., GOLEM-EV, GOLEM-NV, NOTEARS-L1 and NOTEARS) on ER graphs are reported in Figure 1, while complete results can be found in Appendix G.2. One first observes that gradient-based methods consistently outperform the other methods. Among gradient-based methods, GOLEM-EV and GOLEM-NV have the best performance in most settings,

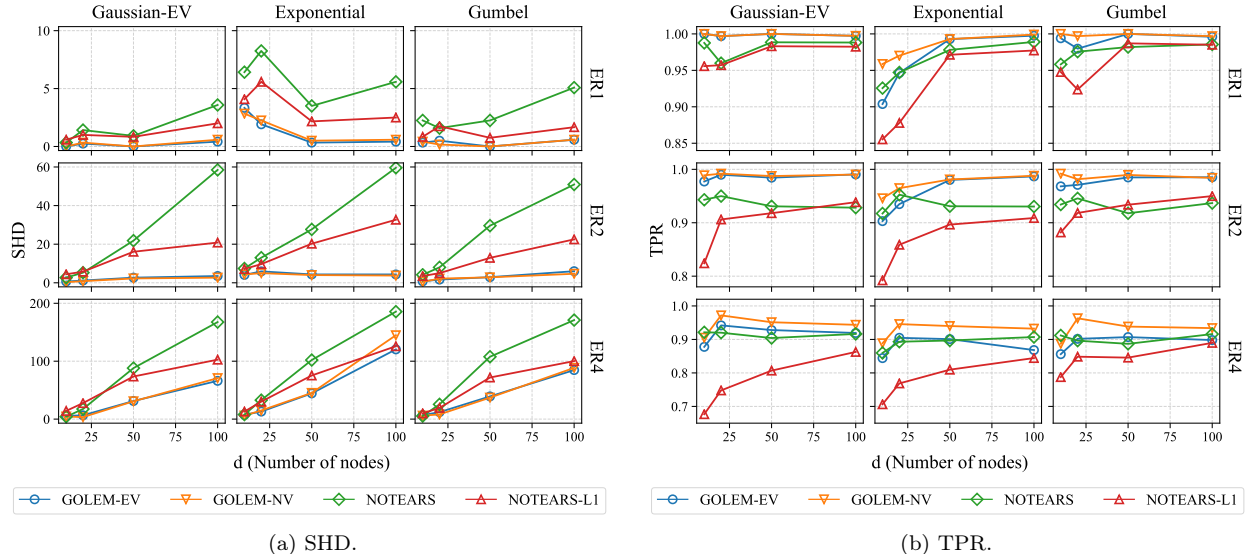


Figure 1: Results in terms of SHD (lower is better) and TPR (higher is better) on ER graphs, with sample size  $n = 1000$ . Rows: graph types with different edge density. Columns: noise types. Since each panel has a number of lines, for clarity we do not provide the standard deviation here.

especially on large graphs. Surprisingly, these two methods perform well even in non-Gaussian cases, i.e., *Exponential* and *Gumbel* noises, although they are based on Gaussian likelihood. We suspect that the number of edges whose directions cannot be determined is not high, giving rise to a high accuracy of our methods even in terms of SHDs of the DAGs. Consistent with previous work, FGS and DirectLiNGAM are competitive on sparse graphs (ER1), but their performance degrades as the edge density and graph size increase.

### 5.3 Numerical Results: Non-Identifiable Cases

We now conduct experiments on the non-identifiable cases, by considering the general linear Gaussian setting (i.e., *Gaussian-NV*). We simulate {ER1, ER2, ER4} graphs with graph size  $d \in \{10, 20, 50, 100\}$ . Hereafter, we only compare with NOTEARS-L1, as it is the best performing baseline in the previous experiment.

Due to limited space, the results are given in Appendix G.3. Not surprisingly, GOLEM-NV shows significant improvements over GOLEM-EV in most settings, as the assumption of equal noise variances does not hold here. It also outperforms NOTEARS-L1 by a large margin on denser graphs, such as ER2 and ER4 graphs. Although GOLEM-EV and NOTEARS-L1 both assume equal noise variances (which does not hold here), it is interesting to observe that they excel in different settings: NOTEARS-L1 demonstrates outstanding performance on sparse graphs (ER1), but deteriorates on ER4 graphs, and vice versa for GOLEM-EV.

### 5.4 Scalability and Optimization Time

We compare the scalability of GOLEM-EV with NOTEARS-L1 on ER2 graphs with  $d \in \{50, 100, 200, \dots, 1600\}$  nodes and *Gaussian-EV* noise. Due to the long optimization time, we were only able to scale NOTEARS-L1 up to 800 nodes. The experiments of GOLEM-EV were computed on the P3 instance hosted on Amazon Web Services with NVIDIA V100 Tensor Core GPU and 16GB of memory, while NOTEARS-L1 were benchmarked using the F4 instance on Microsoft Azure with four 2.4 GHz Intel Xeon CPU cores and 8GB of memory.<sup>4</sup>

<sup>4</sup>For NOTEARS-L1, we have experimented with more CPU cores, such as the F16 instance on Microsoft Azure with sixteen CPU cores and 32GB of memory, but there is only minor improvement in the optimization time.

On graphs of 1600 nodes, the optimization of GOLEM can be unstable due to the large search space and insufficient sample size, hence we use a simple heuristic to pick the final graph based on likelihood value (cf. Appendix E). Figure 8 in Appendix G.4 shows that GOLEM-EV remains competitive on large graphs, with SHD lower than 30 and 60 on graphs of 400 and 800 nodes, respectively. By contrast, the performance of NOTEARS-L1 degrades as the graph size increases, which may be attributed to the unstable behaviors of constrained optimization (cf. Section 2.2). There is a slight drop in the performance of GOLEM-EV on 1600-node graphs, possibly because of the insufficient sample size (i.e.,  $n = 1000$ ).

As depicted in Figure 9, the average optimization time of NOTEARS-L1 scales superlinearly, which is consistent with the  $\mathcal{O}(d^3)$  evaluation cost of matrix exponential (Zheng et al., 2018). Despite also requiring  $\mathcal{O}(d^3)$  cost per iteration, GOLEM-EV takes a much shorter time especially on large graphs, with approximately linear growth of optimization time. This is because the optimization of GOLEM-EV is highly parallelizable on GPU, showing that the cubic cost is not a major concern. We believe that the optimization of NOTEARS-L1 could also be accelerated in a similar fashion.

## 5.5 Sensitivity Analysis of Weight Scale

We investigate the sensitivity to weight scaling, as in (Zheng et al., 2018). We consider 50-node ER2 graphs with *Gaussian-EV* noise and edge weights sampled uniformly from  $\alpha \cdot [-2, -0.5] \cup \alpha \cdot [0.5, 2]$  where  $\alpha \in \{0.3, 0.4, \dots, 1.0\}$ . The threshold  $\omega$  is set to 0.1 for both GOLEM-EV and NOTEARS-L1 in this analysis.

The complete results are provided in Appendix G.5. One first observes that GOLEM-EV has consistently low SHDs and high TPRs, indicating that our method is robust to different weight scales. By contrast, the performance of NOTEARS-L1 is unstable across different weight scales: it has low TPRs on small weight scales, and high FDRs on large ones, resulting in the “U-shaped” SHD curve. A possible reason of the low TPRs is that the signal-to-noise ratio decreases when the weight scales are small, whereas for large weight scales, NOTEARS-L1 may have multiple edges with intermediate values, resulting in the high FDRs.

## 5.6 Real Data

We also compare the proposed method with NOTEARS-L1 on a real dataset which measures the expression levels of proteins and phospholipids in human cells (Sachs et al., 2005). This dataset is commonly used in the literature of probabilistic graphical models, with experimental annotations accepted by the biological community. Based on  $d = 11$  cell types and  $n = 853$  observational samples, the ground truth structure given by Sachs et al. (2005) contains 17 edges. On this dataset, GOLEM-NV achieves the best SHD 14 with 11 estimated edges. NOTEARS-L1 is on par with GOLEM-NV with an SHD of 15 and 13 total edges, while GOLEM-EV estimated 21 edges with an SHD of 18.

## 6 Conclusion

In this work, we investigated whether the hard DAG constraint used by Zheng et al. (2018), and another widely used sparsity constraint, are necessary for learning linear DAGs. In particular, we studied the asymptotic roles of the sparsity and DAG constraints in the general linear Gaussian case, as well as other specific cases including the linear non-Gaussian model and linear Gaussian model with equal noise variances. We also investigated their usefulness in the finite sample regime. Our theoretical results suggest that when the optimization problem is formulated using the likelihood-based objective in place of least squares, one only has to apply sparsity and DAG regularization terms to recover the underlying DAGs. This removes the need for a hard DAG constraint and is easier to solve. As a by-product, we developed a likelihood-based structure learning method with continuous optimization, and demonstrated its effectiveness through extensive experiments in both identifiable and non-identifiable cases. The resulting score-based method can easily handle thousand of nodes while retaining a high accuracy. Future work include extending the current procedure to other score function, such as BDe (Heckerman et al., 1995), decreasing the optimization time via deploying a proper early stopping criterion, and devising a systematic way to pick the value of  $\omega$  for thresholding.

## References

M. Abadi, P. Barham, Z. Chen, Jianminand Chen, A. Davis, J. Dean, M. Devin, S. Ghemawat, G. Irving, M. Isard, et al. Tensorflow: A system for large-scale machine learning. In *12th USENIX Symposium on Operating Systems Design and Implementation (OSDI)*, 2016.

A. Al-Mohy and N. Higham. A new scaling and squaring algorithm for the matrix exponential. *SIAM Journal on Matrix Analysis and Applications*, 31, 2009.

B. Aragam and Q. Zhou. Concave penalized estimation of sparse gaussian Bayesian networks. *Journal of Machine Learning Research*, 16(1):2273–2328, 2015.

A.-L. Barabási and R. Albert. Emergence of scaling in random networks. *Science*, 286(5439):509–512, 1999.

D. P. Bertsekas. *Nonlinear Programming*. Athena Scientific, 1999.

E. G. Birgin, R. A. Castillo, and J. M. Martínez. Numerical comparison of augmented lagrangian algorithms for nonconvex problems. *Computational Optimization and Applications*, 31:31–55, 2005.

E. G. Birgin, D. Fernández, and J. M. Martínez. The boundedness of penalty parameters in an augmented lagrangian method with constrained subproblems. *Optimization Methods and Software*, 27(6):1001–1024, 2012.

R. Byrd, P. Lu, J. Nocedal, and C. Zhu. A limited memory algorithm for bound constrained optimization. *SIAM Journal on Scientific Computing*, 16, 2003.

D. M. Chickering. Learning Bayesian networks is NP-complete. In *Learning from Data: Artificial Intelligence and Statistics V*. Springer, 1996.

D. M. Chickering. Optimal structure identification with greedy search. *Journal of Machine Learning Research*, 3(Nov):507–554, 2002.

D. Colombo, M. Maathuis, M. Kalisch, and T. Richardson. Learning high-dimensional directed acyclic graphs with latent and selection variables. *The Annals of Statistics*, 40:294–321, 2011.

P. Erdős and A. Rényi. On random graphs I. *Publicationes Mathematicae*, 6:290–297, 1959.

J. Friedman, T. Hastie, and R. Tibshirani. Sparse inverse covariance estimation with the graphical lasso. *Biostatistics*, 9:432–41, 2008.

A. Ghassami, K. Zhang, and N. Kiyavash. Characterizing distribution equivalence for cyclic and acyclic directed graphs. *arXiv preprint arXiv:1910.12993*, 2019.

I. Han, D. Malioutov, and J. Shin. Large-scale log-determinant computation through stochastic chebyshev expansions. In *International Conference on Machine Learning*, 2015.

Y. He, J. Jia, and B. Yu. Counting and exploring sizes of markov equivalence classes of directed acyclic graphs. *Journal of Machine Learning Research*, 16:2589–2609, 2015.

D. Heckerman, D. Geiger, and D. Chickering. Learning Bayesian networks: The combination of knowledge and statistical data. *Machine Learning*, 20:197–243, 1995.

A. Hyvärinen, J. Karhunen, and E. Oja. *Independent Component Analysis*. John Wiley & Sons, Inc, 2001.

D. Kalainathan, O. Goudet, I. Guyon, D. Lopez-Paz, and M. Sebag. Structural agnostic modeling: Adversarial learning of causal graphs. *arXiv preprint arXiv:1803.04929*, 2018.

D. Kingma and J. Ba. Adam: A method for stochastic optimization. In *International Conference on Learning Representations*, 2014.

D. Koller and N. Friedman. *Probabilistic Graphical Models: Principles and Techniques*. MIT Press, Cambridge, MA, 2009.

S. Lachapelle, P. Brouillard, T. Deleu, and S. Lacoste-Julien. Gradient-based neural DAG learning. In *International Conference on Learning Representations*, 2020.

P. J. F. Lucas, L. C. van der Gaag, and A. Abu-Hanna. Bayesian networks in biomedicine and healthcare. *Artificial Intelligence in Medicine*, 30(3):201–214, 2004.

N. Meinshausen and P. Bühlmann. High-dimensional graphs and variable selection with the Lasso. *The Annals of Statistics*, 34:1436–1462, 2006.

I. Ng, Z. Fang, S. Zhu, Z. Chen, and J. Wang. Masked gradient-based causal structure learning. *arXiv preprint arXiv:1910.08527*, 2019a.

I. Ng, S. Zhu, Z. Chen, and Z. Fang. A graph autoencoder approach to causal structure learning. *arXiv preprint arXiv:1911.07420*, 2019b.

Y. Nie, H. Zhang, and D.-H. Lee. Models and algorithms for the traffic assignment problem with link capacity constraints. *Transportation Research Part B: Methodological*, 38(4):285–312, 2004.

R. Pamfil, N. Sriwattanaworachai, S. Desai, P. Pilgerstorfer, P. Beaumont, K. Georgatzis, and B. Aragam. DYNOTEARS: Structure learning from time-series data. In *International Conference on Artificial Intelligence and Statistics*, 2020.

J. Pearl. *Causality: Models, Reasoning and Inference*. Cambridge University Press, 2009.

J. Peters and P. Bühlmann. Identifiability of gaussian structural equation models with equal error variances. *Biometrika*, 101(1):219–228, 2013.

J. Ramsey, M. Glymour, R. Sanchez-Romero, and C. Glymour. A million variables and more: the fast greedy equivalence search algorithm for learning high-dimensional graphical causal models, with an application to functional magnetic resonance images. *International Journal of Data Science and Analytics*, 3(2):121–129, 2017.

G. Raskutti and C. Uhler. Learning directed acyclic graph models based on sparsest permutations. *Stat*, 7(1):e183, 2018.

T. Richardson. A polynomial-time algorithm for deciding markov equivalence of directed cyclic graphical models. In *Conference on Uncertainty in Artificial Intelligence*, pages 462–469, 1996.

K. Sachs, O. Perez, D. Pe’er, D. A. Lauffenburger, and G. P. Nolan. Causal protein-signaling networks derived from multiparameter single-cell data. *Science*, 308(5721):523–529, 2005.

G. Schwarz. Estimating the dimension of a model. *The Annals of Statistics*, 6(2):461–464, 1978.

S. Shimizu, P. O. Hoyer, A. Hyvärinen, and A. Kerminen. A linear non-Gaussian acyclic model for causal discovery. *Journal of Machine Learning Research*, 7(Oct):2003–2030, 2006.

S. Shimizu, T. Inazumi, Y. Sogawa, A. Hyvärinen, Y. Kawahara, T. Washio, P. O. Hoyer, and K. Bollen. Directlingam: A direct method for learning a linear non-Gaussian structural equation model. *Journal of Machine Learning Research*, 12(Apr):1225–1248, 2011.

L. Solus, Y. Wang, L. Matejovicova, and C. Uhler. Consistency guarantees for permutation-based causal inference algorithms. *arXiv preprint arXiv:1702.03530*, 2017.

P. Spirtes and C. Glymour. An algorithm for fast recovery of sparse causal graphs. *Social Science Computer Review*, 9:62–72, 1991.

P. Spirtes, C. Meek, and T. Richardson. Causal inference in the presence of latent variables and selection bias. In *Conference on Uncertainty in Artificial Intelligence*, 1995.

P. Spirtes, C. Glymour, and R. Scheines. *Causation, Prediction, and Search*. MIT press, 2nd edition, 2000.

V. Strassen. Gaussian elimination is not optimal. *Numer. Math.*, 13(4):354–356, 1969.

M. Teyssier and D. Koller. Ordering-based search: A simple and effective algorithm for learning Bayesian networks. *arXiv preprint arXiv:1207.1429*, 2012.

R. Tibshirani. Regression shrinkage and selection via the lasso. *Journal of the Royal Statistical Society. Series B (Methodological)*, 58(1):267–288, 1996.

S. Van de Geer and P. Bühlmann.  $\ell_0$ -penalized maximum likelihood for sparse directed acyclic graphs. *The Annals of Statistics*, 41(2):536–567, 2013.

Y. Yu, J. Chen, T. Gao, and M. Yu. DAG-GNN: DAG structure learning with graph neural networks. In *International Conference on Machine Learning*, 2019.

X. Zheng, B. Aragam, P. Ravikumar, and E. P. Xing. DAGs with NO TEARS: Continuous optimization for structure learning. In *Advances in Neural Information Processing Systems*, 2018.

X. Zheng, C. Dan, B. Aragam, P. Ravikumar, and E. P. Xing. Learning sparse nonparametric DAGs. In *International Conference on Artificial Intelligence and Statistics*, 2020.

S. Zhu, I. Ng, and Z. Chen. Causal discovery with reinforcement learning. In *International Conference on Learning Representations*, 2020.

## Appendix

### A An Example of Quasi Equivalence

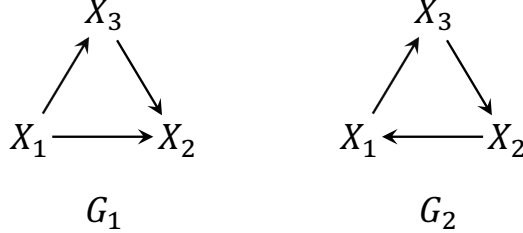


Figure 2: An example of quasi equivalence.

Here, we provide an example of two structures which are quasi equivalent to each other. Consider directed graphs  $G_1$  and  $G_2$  in Figure 2. Since  $G_1$  is a complete DAG, it can generate any precision matrices. Consider an arbitrary precision matrix  $\Theta$  generated by  $G_1$ . If  $\Theta$  is representable by  $G_2$ , then we should be able to decompose it as  $\Theta = QQ^\top$ , where  $Q$  has the following form.

$$Q = \begin{bmatrix} \sigma_1^{-1} & 0 & -\beta_{13}\sigma_3^{-1} \\ -\beta_{21}\sigma_1^{-1} & \sigma_2^{-1} & 0 \\ 0 & -\beta_{32}\sigma_2^{-1} & \sigma_3^{-1} \end{bmatrix}.$$

Therefore, it suffices to show that we have a matrix of form

$$\begin{bmatrix} a & 0 & b \\ c & d & 0 \\ 0 & e & f \end{bmatrix},$$

such that

$$\begin{aligned} a^2 + b^2 &= \Theta_{11} & ac &= \Theta_{12} \\ c^2 + d^2 &= \Theta_{22} & bf &= \Theta_{13} \\ e^2 + f^2 &= \Theta_{33} & de &= \Theta_{23}. \end{aligned}$$

Then we have  $\sigma_1 = a^{-1}$ ,  $\sigma_2 = d^{-1}$ ,  $\sigma_3 = f^{-1}$ ,  $\beta_{13} = -b/f$ ,  $\beta_{21} = -c/a$ ,  $\beta_{32} = -e/d$ .

Suppose the value of  $e$  is fixed. It should satisfy the following constraint:

$$e^2 = \Theta_{33} - \frac{\Theta_{13}^2}{\Theta_{11} - \frac{\Theta_{12}^2}{\Theta_{22} - \frac{\Theta_{23}^2}{e^2}}},$$

or equivalently,

$$(\Theta_{11}\Theta_{22} - \Theta_{12}^2)e^4 + (-\Theta_{11}\Theta_{22}\Theta_{33} - \Theta_{11}\Theta_{23}^2 + \Theta_{22}\Theta_{13}^2 + \Theta_{33}\Theta_{12}^2)e^2 + (\Theta_{11}\Theta_{33}\Theta_{23}^2 - \Theta_{13}^2\Theta_{23}^2) = 0,$$

which does not necessarily have a real root, and only for a non-measure zero subset of the distributions is satisfied.

## B Proofs of Theorems 1 and 2

The following part is required for the proofs of both Theorems 1 and 2:

Let  $G^*$  and  $\Theta$  be the ground truth DAG and the generated distribution (precision matrix). Let  $W$  and  $\Omega$  be the adjacency matrix and the diagonal matrix containing exogenous variances, respectively. Considering weights for regularization terms such that the likelihood term dominates asymptotically, we will find a pair  $(\hat{W}, \hat{\Omega})$ , such that  $(I - \hat{W})\hat{\Omega}^{-1}(I - \hat{W})^\top = \Theta$  and denote the directed graph corresponding to  $\hat{W}$  by  $\hat{G}$ . We have  $\Theta \in \Theta(\hat{G})$ , which implies that  $\Theta$  contains all the distributional constraints of  $\hat{G}$ . Therefore, under the faithfulness assumption, we have  $H(\hat{G}) \subseteq H(G^*)$ . Due to the sparsity regularization we have  $|E(\hat{G})| \leq |E(G^*)|$ , otherwise the algorithm would have outputted  $G^*$ . Therefore, by Assumption 2, we have  $H(\hat{G}) \not\subseteq H(G^*)$ . Now, from  $H(\hat{G}) \subseteq H(G^*)$  and  $H(\hat{G}) \not\subseteq H(G^*)$  we conclude that  $H(\hat{G}) = H(G^*)$ . Therefore,  $\hat{G}$  is quasi equivalent to  $G^*$ .

### Proof of Theorem 1.

To complete the proof of Theorem 1, we show that the output directed graph will be acyclic. We need the notion of virtual edge for the proof: For DAGs, under the Markov and faithfulness assumptions, a variable  $X_i$  is adjacent to a variable  $X_j$  if and only if  $X_i$  and  $X_j$  are dependent conditioned on any subset of the rest of the variables. This is not the case for cyclic directed graphs. Two non-adjacent variables  $X_i$  and  $X_j$  are dependent conditioned on any subset of the rest of the variables if they have a common child  $X_k$  which is an ancestor of  $X_i$  or  $X_j$ . In this case, we say there exists a **virtual edge** between  $X_i$  and  $X_j$  (Richardson, 1996).

We provide a proof by contradiction. Suppose  $\hat{G}$  contains cycles. Suppose  $C = (X_1, \dots, X_c, X_1)$  is a cycle which does not contain any smaller cycles on its vertices. Since  $G^*$  and  $\hat{G}$  should have the same adjacencies (either via a real edge or a virtual edge),  $G^*$  should also have edges in the location of all the edges of  $C$ .

- If  $|C| > 3$ , then the DAG has a v-structure, say,  $X_{i-1} \rightarrow X_i \leftarrow X_{i+1}$ . Therefore, there exists a subset of vertices  $X_S$  such that  $X_i \notin X_S$ , conditioned on which  $X_{i-1}$  and  $X_{i+1}$  are independent. However, this conditional independence relation is not true in  $\hat{G}$ . This contradicts with quasi equivalence.
- If  $|C| = 3$ , then  $G^*$  should also have a triangle on the corresponding three vertices, which contradicts the triangle condition.
- If  $|C| = 2$ , then suppose  $C = (X_1, X_2, X_1)$ . If none of the adjacencies in  $\hat{G}$  to  $C$  are in-going, then  $C$  can be reduced to a single edge and the resulting directed graph is equivalent to  $\hat{G}$  (Ghassami et al., 2019). Hence, due to sparsity regularization, such  $C$  is not possible. If there exists an in-going edge, say from  $X_p$  to one end of  $C$ , there will be a virtual or real edge to the other end of  $C$  as well. Therefore,  $X_p$ ,  $X_1$ , and  $X_2$  are adjacent in  $\hat{G}$  and hence in  $G^*$ , which contradicts the triangle condition. Also, if the edge between  $X_p$  and one end of  $C$  is a virtual edge,  $X_p$  should have a real edge towards another cycle in  $\hat{G}$ , which with the virtual edge, again forms a triangle and hence, again, contradicts the triangle condition.

Therefore, in all cases, quasi equivalence or the triangle assumption is violated, which is a contradiction. Therefore,  $\hat{G}$  is a DAG.  $\square$

### Proof of Theorem 2.

From the first part of the proof, we obtained that  $H(\hat{G}) \subseteq H(G^*)$ . Therefore, by the contrapositive of part (b) of Assumption 2 we have  $|E(\hat{G})| \geq |E(G^*)|$ . Now, due to the sparsity regularization we have  $|E(\hat{G})| \leq |E(G^*)|$ . This concludes that  $|E(\hat{G})| = |E(G^*)|$ .  $\square$

## C Derivations of Maximum Likelihood Objectives

### C.1 Assuming Non-Equal Noise Variances

We start by restating the necessary notations for the derivation. Let  $W$  be a weighted adjacency matrix associated with vertices  $X = [X_1, \dots, X_d]^\top$ , where each node  $X_i$  represents a random variable. The linear DAG model is given by

$$X = W^\top X + Z,$$

where  $Z = [Z_1, \dots, Z_d]^\top \in \mathbb{R}^d$  is a noise vector. Here we assume that the elements of  $Z$  are jointly Gaussian and independent, characterized by the covariance matrix  $\Omega = \text{diag}\{\sigma_1^2, \dots, \sigma_d^2\}$ . Assuming that  $I - W^\top$  is invertible, we rewrite the DAG model as

$$X = (I - W^\top)^{-1}Z.$$

Since one can always center the data, without loss of generality, we assume that  $Z$ , and thus  $X$ , are zero-mean. Therefore, we have  $X \sim \mathcal{N}(0, \Sigma)$  with  $\Sigma$  being the covariance matrix of the multivariate Gaussian distribution on  $X$ . We assume that  $\Sigma$  is always invertible (i.e., the Lebesgue measure of non-invertible matrices is zero). Equivalently, the precision matrix  $\Theta = \Sigma^{-1}$  of  $X$  is given by

$$\Theta = (I - W)\Omega^{-1}(I - W)^\top.$$

The log-density function of  $X$  is then

$$\begin{aligned} \log p_X(x) &= -\frac{1}{2} \log \det \Sigma - \frac{1}{2} x^\top \Theta x - \frac{d}{2} \log(2\pi) \\ &= -\frac{1}{2} \log \det \Omega + \log |\det(I - W)| - \frac{1}{2} x^\top (I - W)\Omega^{-1}(I - W)^\top x + \text{const} \\ &= -\sum_{i=1}^d \log \sigma_i + \log |\det(I - W)| - \frac{1}{2} \sum_{i=1}^d \frac{(x_i - W_i^\top x)^2}{\sigma_i^2} + \text{const}, \end{aligned}$$

where  $W_i \in \mathbb{R}^d$  denotes the  $i$ -th column vector of  $W$ .

Given i.i.d. samples  $\mathbf{x} = \{x^{(k)}\}_{k=1}^n$  from the joint distribution, the average log-likelihood of  $X$  reads

$$L(\Omega; \mathbf{x}) = -\sum_{i=1}^d \log \sigma_i + \log |\det(I - W)| - \frac{1}{2n} \sum_{i=1}^d \sum_{k=1}^n \frac{(x_i^{(k)} - W_i^\top x^{(k)})^2}{\sigma_i^2} + \text{const.}$$

To compute the maximum likelihood estimate of  $\sigma_i$ , solving  $\frac{\partial L}{\partial \sigma_i} = 0$  yields

$$\hat{\sigma}_i = \sqrt{\frac{1}{n} \sum_{k=1}^n (x_i^{(k)} - W_i^\top x^{(k)})^2}$$

and

$$L(\hat{\Omega}; \mathbf{x}) = -\frac{1}{2} \sum_{i=1}^d \log \left( \sum_{k=1}^n (x_i^{(k)} - W_i^\top x^{(k)})^2 \right) + \log |\det(I - W)| + \text{const.}$$

### C.2 Assuming Equal Noise Variances

If one further assumes that the noise variances are equal, i.e.,  $\sigma_1^2 = \dots = \sigma_d^2 = \sigma^2$ , following similar notations and derivation in Appendix C.1, the log-density function of  $X$  becomes

$$\log p_X(x) = -d \log \sigma + \log |\det(I - W)| - \frac{1}{2\sigma^2} \sum_{i=1}^d (x_i - W_i^\top x)^2 + \text{const},$$

with average log-likelihood

$$L(\Omega; \mathbf{x}) = -d \log \sigma + \log |\det(I - W)| - \frac{1}{2n\sigma^2} \sum_{i=1}^d \sum_{k=1}^n (x_i^{(k)} - W_i^\top x^{(k)})^2 + \text{const.}$$

To compute the maximum likelihood estimate of  $\sigma$ , solving  $\frac{\partial L}{\partial \sigma} = 0$  yields

$$\hat{\sigma} = \sqrt{\frac{1}{n} \sum_{i=1}^d \sum_{k=1}^n (x_i^{(k)} - W_i^\top x^{(k)})^2}$$

and

$$L(\hat{\Omega}; \mathbf{x}) = -\frac{d}{2} \log \left( \sum_{i=1}^d \sum_{k=1}^n (x_i^{(k)} - W_i^\top x^{(k)})^2 \right) + \log |\det(I - W)| + \text{const.}$$

## D Proof of Proposition 1

The following setup is required for the proof of both parts (i) and (ii):

The true weighted adjacency matrix and noise covariance matrix are, respectively,

$$W_0 = \begin{bmatrix} 0 & w_0 \\ 0 & 0 \end{bmatrix}, \Omega = \begin{bmatrix} \sigma^2 & 0 \\ 0 & \sigma^2 \end{bmatrix}, w_0 \neq 0.$$

Note that

$$I - W_0 = \begin{bmatrix} 1 & -w_0 \\ 0 & 1 \end{bmatrix}, (I - W_0)^{-1} = \begin{bmatrix} 1 & w_0 \\ 0 & 1 \end{bmatrix}.$$

In the asymptotic case, the covariance matrix of  $X$  is given by

$$\Sigma = (I - W_0)^{-\top} \Omega (I - W_0)^{-1} = \sigma^2 \begin{bmatrix} 1 & w_0 \\ w_0 & w_0^2 + 1 \end{bmatrix}.$$

Let  $W$  be an off-diagonal matrix defined as

$$W(b, c) = \begin{bmatrix} 0 & b \\ c & 0 \end{bmatrix}.$$

### Proof of part (i).

Plugging  $W(b, c)$  into the least squares objective yields

$$\begin{aligned} \ell(W; \Sigma) &= \text{tr}((I - W)^\top \Sigma (I - W)) \\ &= ((b - w_0)^2 + (w_0 c - 1)^2 + c^2 + 1) \sigma^2. \end{aligned}$$

The contour plot is visualized in Figure 3a. To find stationary points, we solve the following equations:

$$\begin{aligned} \frac{\partial \ell}{\partial b} &= 2(b - w_0)\sigma^2 = 0 & \implies b^* &= w_0, \\ \frac{\partial \ell}{\partial c} &= 2w_0(w_0 c - 1)\sigma^2 + 2c\sigma^2 = 0 & \implies c^* &= \frac{w_0}{w_0^2 + 1}. \end{aligned}$$

Without a DAG constraint, this shows that the least squares objective  $\ell(W; \Sigma)$  will return a cyclic graph  $W\left(w_0, \frac{w_0}{w_0^2 + 1}\right)$ . If one further applies a hard DAG constraint to enforce choosing only one of  $b^*$  and  $c^*$ , we have

$$\ell(W(0, c^*); \Sigma) = \left( w_0^2 + 1 + \frac{1}{w_0^2 + 1} \right) \sigma^2 > 2\sigma^2 = \ell(W(b^*, 0); \Sigma),$$

where the inequality follows from the AM-GM inequality and  $w_0 \neq 0$ . Therefore, under a hard DAG constraint,  $W(w_0, 0)$  is asymptotically the unique minimizer of the least squares objective  $\ell(W; \Sigma)$ .

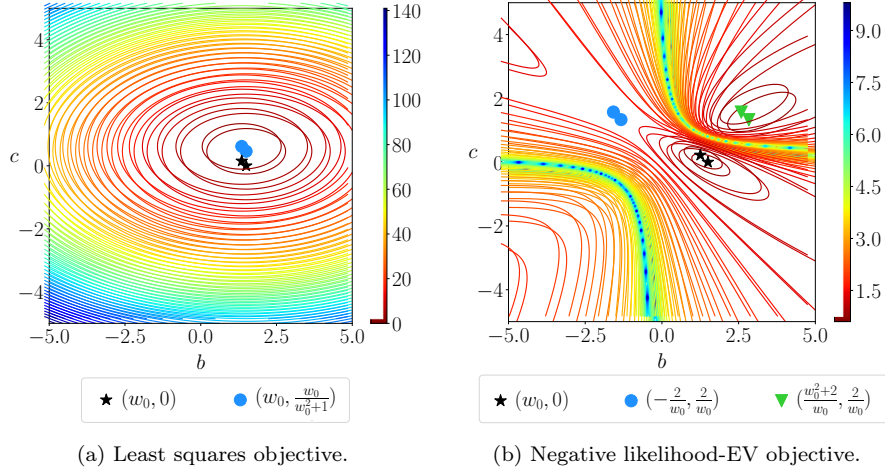


Figure 3: The contour plot of different objectives in the bivariate case (with  $w_0 = 1.5$  and  $\sigma = 1.0$ ). Lower is better. The black star corresponds to the ground truth DAG  $W(w_0, 0)$ , while the blue circle and green triangle indicate the (other) stationary solution(s).

### Proof of part (ii).

Plugging  $W(b, c)$  into the negative likelihood-EV objective (3) yields

$$\begin{aligned} -\mathcal{L}_2(W; \Sigma) &= \log \left( \text{tr} \left( (I - W)^T \Sigma (I - W) \right) \right) - \log |\det(I - W)| \\ &= \log \left( (b - w_0)^2 + (w_0 c - 1)^2 + c^2 + 1 \right) \sigma^2 - \log |1 - bc|, \end{aligned}$$

with contour plot depicted in Figure 3b. To find stationary points, we solve the following equations:

$$\begin{aligned} \frac{\partial \mathcal{L}_2}{\partial b} &= \frac{2(b - w_0)}{(b - w_0)^2 + (w_0 c - 1)^2 + c^2 + 1} + \frac{c}{1 - bc} = 0, \\ \frac{\partial \mathcal{L}_2}{\partial c} &= \frac{2w_0(w_0 c - 1) + 2c}{(b - w_0)^2 + (w_0 c - 1)^2 + c^2 + 1} + \frac{b}{1 - bc} = 0. \end{aligned}$$

Further algebraic manipulations yield three stationary solutions and their respective objective values:

$$\begin{cases} b^* = w_0, c^* = 0 & \implies -\mathcal{L}_2(W(b^*, c^*); \Sigma) = \log 2 + \log \sigma^2 \\ b^* = \frac{w_0^2 + 2}{w_0}, c^* = \frac{2}{w_0} & \implies -\mathcal{L}_2(W(b^*, c^*); \Sigma) = \log 2 + \log \sigma^2 \\ b^* = -\frac{2}{w_0}, c^* = \frac{2}{w_0} & \implies -\mathcal{L}_2(W(b^*, c^*); \Sigma) = \log(2 + w_0^2) + \log \sigma^2. \end{cases}$$

Clearly, the two minimizers are  $W(w_0, 0)$  and  $W\left(\frac{w_0^2+2}{w_0}, \frac{2}{w_0}\right)$ . With DAG regularization, the cyclic solution  $W\left(\frac{w_0^2+2}{w_0}, \frac{2}{w_0}\right)$  is penalized; thus, the acyclic solution  $W(w_0, 0)$  becomes the unique minimizer of the objective  $-\mathcal{L}_2(W; \Sigma)$ . For  $\ell_1$  regularization, we have that

$$\left\| W\left(\frac{w_0^2+2}{w_0}, \frac{2}{w_0}\right) \right\|_1 = \left| \frac{w_0^2+2}{w_0} \right| + \left| \frac{2}{w_0} \right| = \frac{w_0^2+4}{|w_0|} > |w_0| = \|W(w_0, 0)\|_1.$$

Hence, similar to DAG regularization,  $\ell_1$  regularization encourages the desired solution  $W(w_0, 0)$  and makes it asymptotically the unique minimizer of the negative likelihood-EV objective  $-\mathcal{L}_2(W; \Sigma)$ .  $\square$

## E Optimization Procedure and Hyperparameters

We restate the unconstrained optimization problems here:

$$\min_W \mathcal{S}_i(W; \mathbf{x}) = -\mathcal{L}_i(W; \mathbf{x}) + \lambda_1 \|W\|_1 + \lambda_2 h(W),$$

where  $i = 1, 2$ ,  $\mathcal{L}_1(W; \mathbf{x})$  and  $\mathcal{L}_2(W; \mathbf{x})$  are the likelihood-based objectives assuming non-equal and equal noise variances, respectively,  $h(W) := \text{tr}(e^{W \odot W}) - d$  is the DAG regularization term. We always set the diagonal entries of  $W$  to be 0 to avoid self-loops. The optimization problem is solved using gradient descent implemented in `Tensorflow` (Abadi et al., 2016) with automatic differentiation and Adam optimizer (Kingma and Ba, 2014). The Adam optimizer is one of the most commonly used gradient descent algorithm for deep learning as it requires less fine-tuning on the learning rate. We use a small learning rate  $1 \times 10^{-3}$  and train for  $1 \times 10^5$  iterations to ensure convergence. The optimization iterations could be decreased via deploying a larger learning rate or proper early stopping criterion, which is left for future investigation. Note that all samples  $\{x^{(k)}\}_{k=1}^n$  are used to estimate the gradient. If they cannot be loaded at once into the memory, we may use stochastic gradient descent by sampling mini-batch in each iteration for gradient estimation.

In practice, one should use cross-validation to select the regularization coefficients. Here we simply pick small values for them, i.e.,  $\lambda_1 = 2 \times 10^{-2}$  and  $\lambda_2 = 5.0$  for GOLEM-EV;  $\lambda_1 = 2 \times 10^{-3}$  and  $\lambda_2 = 5.0$  for GOLEM-NV. Unless otherwise stated, after the optimization ends, we apply a thresholding step at  $\omega = 0.3$ , then remove edges iteratively starting from the smallest absolute weights, until a DAG is obtained (cf. Section 4.2).

On graphs of 1600 nodes, the optimization of GOLEM-EV can be unstable due to the large search space and insufficient sample size  $n = 1000$ ; hence, we use a simple heuristic for graph selection. In the final 10000 iterations of the optimization, we check the log-likelihood value periodically every 2000 iterations and pick the graph with the best likelihood. This heuristic is not needed for graphs with equal or smaller than 800 nodes.

## F Supplementary Experiment Details

### F.1 Implementation of Baselines

We use existing implementations of structure learning methods in comparison, as listed below:

- FGS: It was implemented through the `py-causal` package, available at <https://github.com/bd2kccd/py-causal>. We adopt `cg-bic-score` as it gives better performance than the `sem-bic-score`.
- PC: It was implemented through the `py-causal` package with Fisher Z-tests, available at <https://github.com/bd2kccd/py-causal>.
- DirectLiNGAM: Its Python implementation is available at the first author’s GitHub repository <https://github.com/cdt15/lingam>.
- NOTEARS: We compare with two variants with or without  $\ell_1$  regularization, denoted as NOTEARS-L1 and NOTEARS, respectively. Regarding the choice of  $\ell_1$  regularization coefficient, we found that the default choice  $\lambda = 0.1$  in the author’s code provides better performance than that of  $\lambda = 0.5$  used in their paper; we therefore treat NOTEARS-L1 favorably by picking  $\lambda$  to be 0.1. Note that cycles may still exist after thresholding at  $\omega = 0.3$ ; thus, a similar post-processing step described in Section 4.2 is taken to obtain DAGs. The codes are available at the first author’s GitHub repository <https://github.com/xunzheng/notears>.

In the experiments, we use default hyperparameters for these baselines unless otherwise stated.

## F.2 Experiment Setup

The experiment setup is similar to (Zheng et al., 2018). We consider two random graph models:

- *Erdős–Rényi* (ER) graphs (Erdős and Rényi, 1959) are generated by adding edges independently with equal probability  $p = \frac{2e}{d^2-d}$ , where  $e$  is the expected number of edges in the resulting graph. For each  $d$ -node graph, we simulate graphs with  $e$  equals to  $d$ ,  $2d$  or  $4d$ , denoted by ER1, ER2 and ER4, respectively.
- *Scale Free* (SF) graphs are simulated using the Barabási-Albert model (Barabási and Albert, 1999), which is based on the preferential attachment process, with nodes being added sequentially. In particular,  $m$  edges are added each time between the new node and existing nodes (with  $m$  equals to 1, 2 or 4), denoted by SF1, SF2 and SF4, respectively.

Based on the DAG sampled from one of the two graph models, we assign edge weights sampled independently from Uniform  $([-2, -0.5] \cup [0.5, 2])$  to construct the weighted adjacency matrix  $W \in \mathbb{R}^{d \times d}$ . The observational data  $\mathbf{x}$  is then generated according to the linear DAG model (cf. Section 2.1) with different graph sizes  $d \in \{10, 20, 50, 100\}$ , and additive noise types:

- *Gaussian-EV* (equal variances).  $Z_i \sim \mathcal{N}(0, 1)$ ,  $i = 1, \dots, d$ .
- *Exponential*.  $Z_i \sim \text{Exp}(1)$ ,  $i = 1, \dots, d$ .
- *Gumbel*.  $Z_i \sim \text{Gumbel}(0, 1)$ ,  $i = 1, \dots, d$ .
- *Gaussian-NV* (non-equal variances).  $Z_i \sim \mathcal{N}(0, \sigma_i^2)$ ,  $i = 1, \dots, d$ , where  $\sigma_i \sim \text{Uniform}[1, 2]$ .

The first three noise models are known to be identifiable in the linear case. Unless otherwise stated, we generate  $n = 1000$  samples for each of these settings.

## F.3 Metrics

We evaluate the estimated graphs using four different metrics:

- **Structural Hamming Distance (SHD)** indicates the number of edge additions, deletions, and reversals in order to transform the estimated graph into the ground truth DAG.
- **True Positive Rate (TPR)** measures the proportion of actual positive edges that are correctly identified as such.
- **False Discovery Rate (FDR)** measures the proportion of false discoveries among the estimated edges.
- **SHD-CPDAG** is very similar to SHD. The only difference is that both estimated graphs and ground truth DAGs are first mapped to their corresponding CPDAGs before calculating SHD. This metric evaluates the performance on recovering the Markov equivalence class. We use a Python implementation through the `CausalDiscoveryToolbox` package, available at <https://github.com/FenTechSolutions/CausalDiscoveryToolbox>.

All experiment results involving synthetic data are averaged over 12 random seeds. Note that PC and FGS output a CPDAG instead of a DAG, which may contain undirected edges. We therefore treat them favorably by considering undirected edges as true positives if the true graph has a directed edge in place of the undirected ones.

## G Supplementary Experiment Results

### G.1 Asymptotic Roles of Sparsity and DAG Constraints

This section provides additional results on the asymptotic roles of sparsity and DAG regularizations terms in Section 5.1, as shown in Figure 4 and 5. For both figures, lower is better, except for TPR.

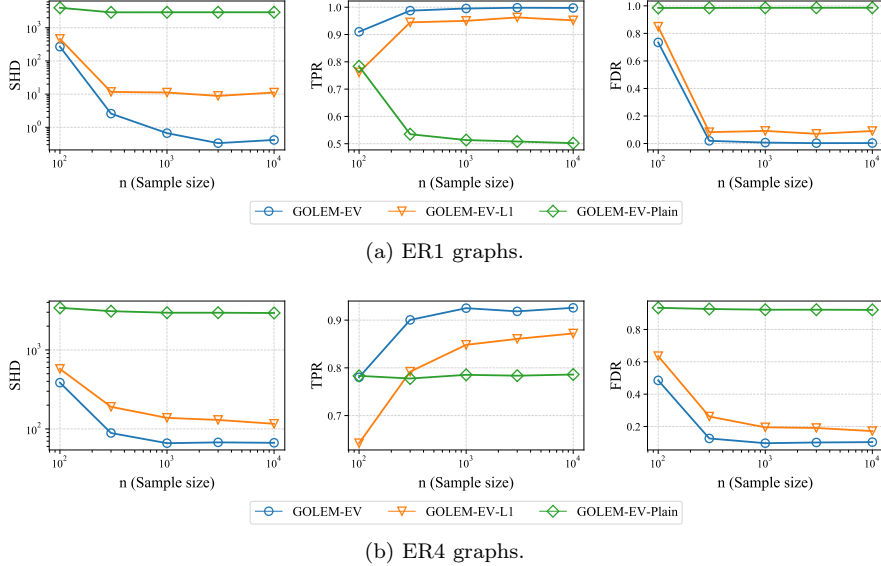


Figure 4: Results on different sample sizes, in the identifiable case (i.e., *Gaussian-EV*). Different variants are compared: GOLEM-EV (with  $\ell_1$  and DAG regularizations), GOLEM-EV-L1 (with only  $\ell_1$  regularization) and GOLEM-EV-Plain (without any regularization term). The  $x$ -axes and SHD are visualized in log scale.

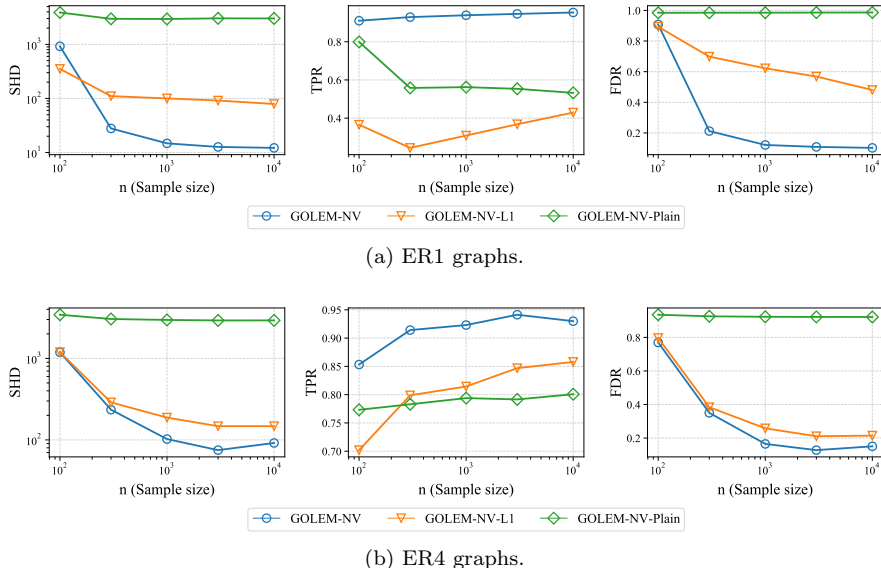


Figure 5: Results on different sample sizes, in the non-identifiable case (i.e., *Gaussian-NV*). Different variants are compared: GOLEM-NV (with  $\ell_1$  and DAG regularizations), GOLEM-NV-L1 (with only  $\ell_1$  regularization) and GOLEM-NV-Plain (without any regularization term). The  $x$ -axes and SHD are visualized in log scale.

## G.2 Numerical Results: Identifiable Cases

This section provides additional results in the identifiable cases (for Section 5.2), as shown in Figure 6. For DirectLiNGAM, we only report its performance on the linear DAG model with *Exponential* and *Gumbel* noises, since its accuracy is significantly lower than the other methods on *Gaussian-EV* noise.

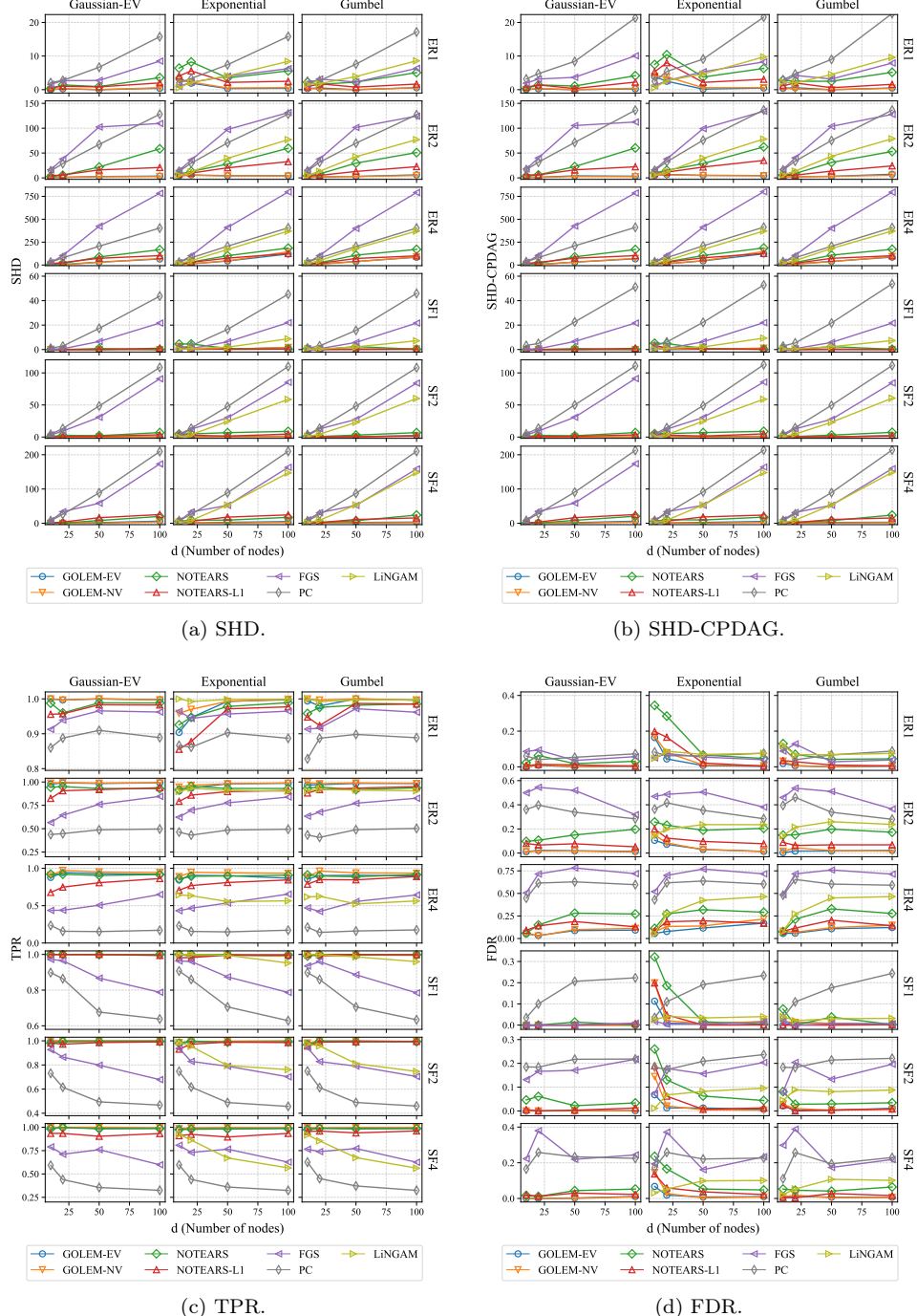


Figure 6: Results in the identifiable cases, with sample size  $n = 1000$ . Lower is better, except for TPR (lower left). Rows: graph types with different edge density. Columns: noise types.

### G.3 Numerical Results: Non-Identifiable Cases

This section provides additional results in the non-identifiable cases (for Section 5.3), as shown in Figure 7.

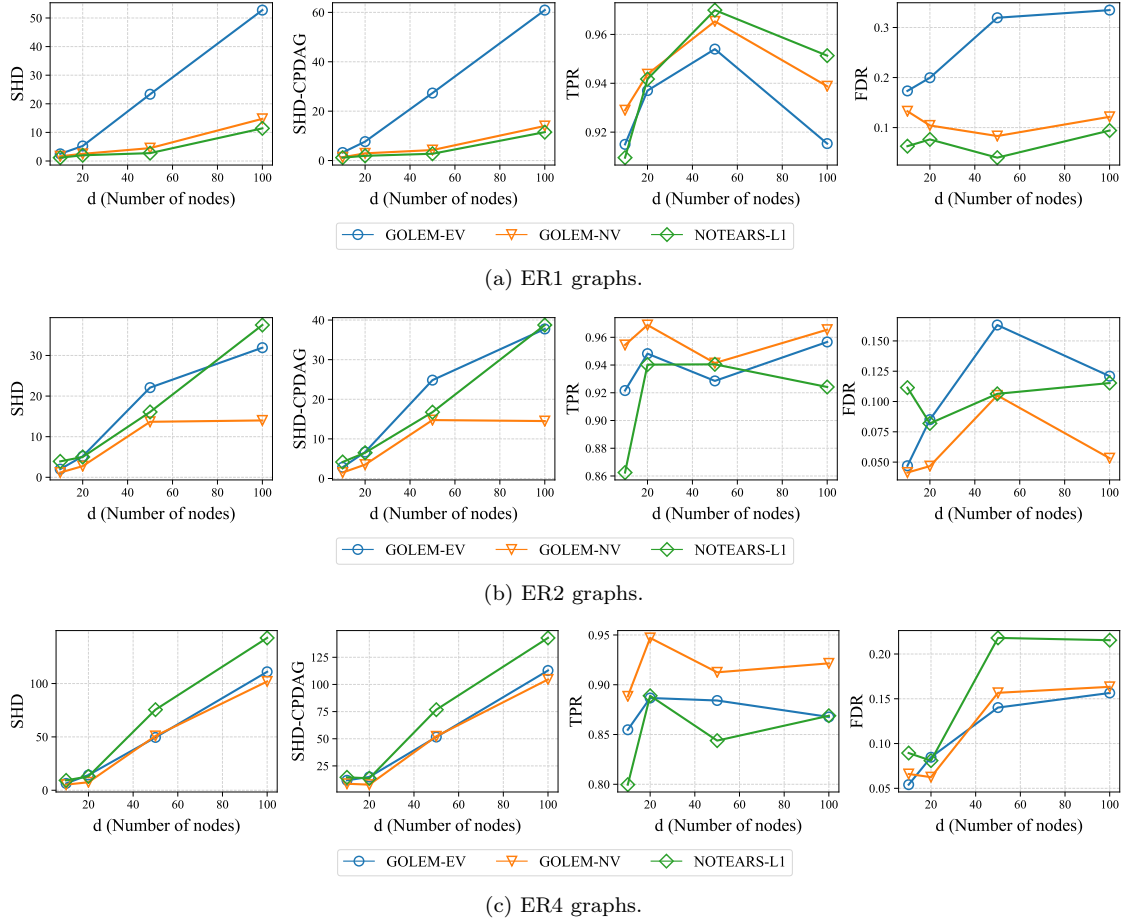


Figure 7: Results in the non-identifiable case (i.e., *Gaussian-NV*), with sample size  $n = 1000$ . Lower is better, except for TPR. Experiments are conducted on graphs with different edge density, namely, ER1, ER2 and ER4 graphs.

## G.4 Scalability and Optimization Time

This section provides additional results for investigating the scalability and optimization time in Section 5.4. The structure learning results and optimization time are reported in Figure 8 and 9, respectively.

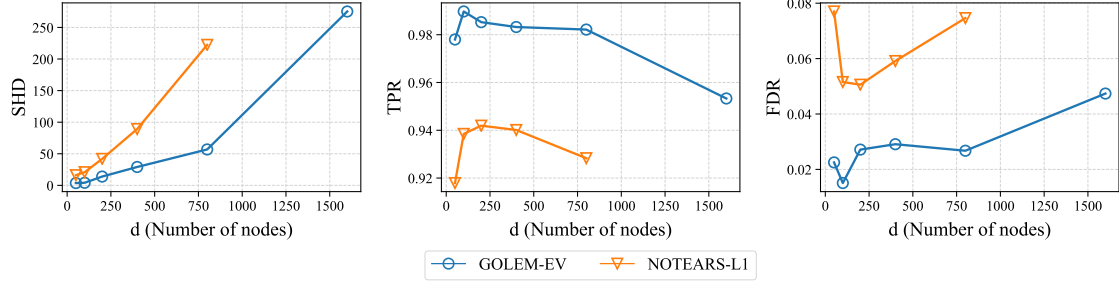


Figure 8: Results on large ER2 graphs, in the identifiable case (i.e., *Gaussian-EV*), with sample size  $n = 1000$ . Lower is better, except for TPR. Due to the long optimization time, we were only able to scale NOTEARS-L1 up to 800 nodes.

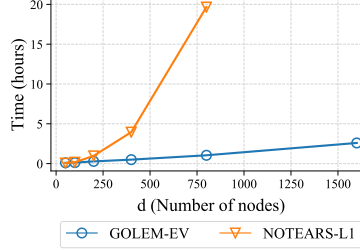


Figure 9: Optimization time on large ER2 graphs, in the identifiable case (i.e., *Gaussian-EV*), with sample size  $n = 1000$ . Lower is better. Due to the long optimization time, we were only able to scale NOTEARS-L1 up to 800 nodes.

## G.5 Sensitivity Analysis of Weight Scale

This section provides additional results on the sensitivity analysis to weight scaling in Section 5.5, as shown in Figure 10.

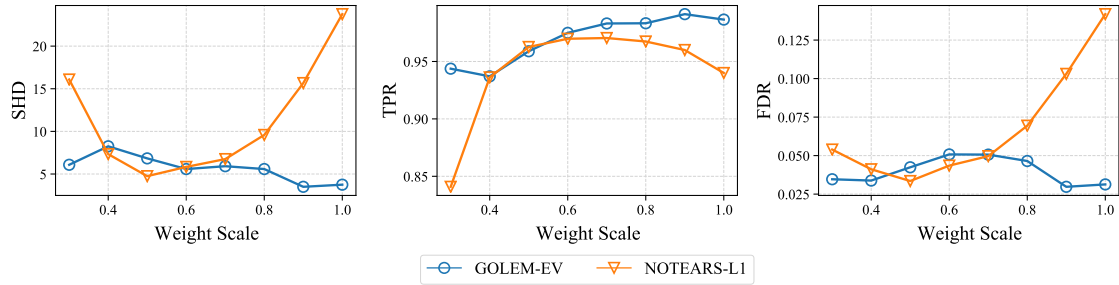


Figure 10: Results on different weight scales, in the identifiable case (i.e., *Gaussian-EV*), with sample size  $n = 1000$ . Lower is better, except for TPR.